ELSEVIER

## Contents lists available at ScienceDirect

## Ultramicroscopy

journal homepage: www.elsevier.com/locate/ultramic



# SimulaTEM: Multislice simulations for general objects

A. Gómez-Rodríguez\*, L.M. Beltrán-del-Río, R. Herrera-Becerra

Departamento de Materia Condensada, Instituto de Física, Universidad National Autónoma de México, México, D.F. C.P. 04510, Mexico

#### ARTICLE INFO

Article history:
Received 3 November 2008
Received in revised form
26 August 2009
Accepted 22 September 2009

Keywords:
Electron diffraction
Multislice
Image simulation
High resolution electron microscopy

#### ABSTRACT

In this work we present the program SimulaTEM for the simulation of high resolution micrographs and diffraction patterns. This is a program based on the multislice approach that does not assume a periodic object. It can calculate images from finite objects, from amorphous samples, from crystals, quasicrystals, grain boundaries, nanoparticles or arbitrary objects provided the coordinates of all the atoms can be supplied.

© 2009 Elsevier B.V. All rights reserved.

## 1. Introduction

Electron microscope images are aberrated interference patterns arising in a complex way from the electron-sample interaction. For this reason direct interpretation from the micrographs is seldom feasible, instead one has to perform simulations, compare them with the actual micrographs and, if there is no reasonable agreement, to modify the theoretical model and run the simulation again till some reasonable match is achieved between observed and calculated images. The multislice method of Cowley and Moodie [1] is, surely, the most widely used method for the simulation of high resolution images. However, most implementations have in mind periodic objects, for instance the space group is required. In this work we present a program, SimulaTEM, based on the multislice scheme, that can calculate images and diffraction patterns from arbitrary objects. The input to the program is the list of all the atomic positions and atomic numbers. In this way nanocrystals, grain boundaries, amorphous objects, large or small molecules etc. can be simulated. Of course the program can also simulate images of crystals but for this purpose there are better programs. Since discrete Fourier transforms are used, there is a form of periodicity implied: that of the "supercell" comprising the whole object.

Among the practical advantages of SimulaTEM are: (1) It is a small program (seven files, 928 KB). (2) It does not require installation other than copying the files into a suitable folder. (3) It does not write into the registry. (4) It can be run from an USB

memory unit, it is truly "portable". The program was specifically written for the Windows platform and it cannot be used with other operating systems.

## 2. Multislice method

Not surprisingly, the starting point is Schrödinger's equation which we have written in the usual way

$$\nabla^2 \phi + \left(\frac{2m}{\hbar^2}\right)(E - V)\phi = 0 \tag{1}$$

notice that here V is the potential energy of the electron (say, in Joules or electron volts) and NOT the electric potential  $\mathcal{V}$ , both being related by means  $V=-e\mathcal{V}$ ; consequently, some readers might feel that a factor -e is missing in many of the equations below

In SimulaTEM we have used the multislice method of Cowley and Moodie [1], for a review of all the relevant ideas and techniques the reader should see the book by Kirkland [2] and also the review by Ishuzuka [3]. It is based on considering the sample (that can be crystalline, quasicrystalline, amorphous etc.) as divided into slices of thickness  $\Delta z$  (z is also the direction of the normal to the slices and is the direction of the optical axis of the microscope). For every slice, the amplitude leaving the slice  $\phi_n$  is given in terms of the amplitude  $\phi_{(n-1)}$  entering it by

$$\phi_n = T_n(\phi_{n-1} * P_{\Delta z}(x, y)) \tag{2}$$

where the transmission function  $T_n$  for slice n is given by

$$T_n = e^{-i\sigma V_p^n(x,y)} \tag{3}$$

<sup>\*</sup> Corresponding author. *E-mail address:* alfredo@fisica.unam.mx (A. Gómez-Rodríguez).

Here \* represents a convolution,  $V_p^n(x,y,z)$  is the projected potential of the n-th slice

$$V_p^n(x,y) = \int_{z_{n-1}}^{z_n} V(x,y,z) \, dz \tag{4}$$

and  $P_{\Delta z}(x,y)$  is the propagator through a distance  $\Delta z$  that (in the paraxial approximation) is

$$P_{\Delta z}(x,y) = \frac{-i}{\lambda} \frac{e^{2\pi i k \Delta z}}{\Delta z} e^{\pi i (x^2 + y^2)/\lambda \Delta z}$$
 (5)

(here the symbols have their standard meaning,  $\lambda$  is the electron wavelength, k is the magnitude of the wave-vector, x and y represent spatial coordinates and  $\sigma$  is the so-called interaction constant, to be defined below).

In this paper all the required convolutions were calculated by means of the convolution theorem using fast Fourier transforms [4].

## 3. Gaussian fitting to atomic factors and projected potential

The present implementation of the multislice method rests upon two steps: the fitting of atomic factors to Gaussian functions and the calculation of the projected potential without assuming periodicity.

In this paper the variable U = (u, v, w) will be used to represent reciprocal space (Fourier space) quantities (spatial frequencies) whereas R = (x, y, z) will be used for ordinary spatial position vectors.

The atomic factors have been expressed as

$$f(U) = \sum_{i=1}^{5} a_i \exp(-b_i U^2)$$
 (6)

where  $a_i$  and  $b_i$  are coefficients to be determined. f(U) is the atomic dispersion factor. Our fit is similar to the one used by

several other authors such as Doyle and Turner [5]. The numerical values for the atomic scattering factors used were those by Cromer and Waber [6]. In our case we found that five Gaussians gave a good precision in the fit. A first approximation was obtained by Klier et al. [7] using the "zxmwd" subroutine of the IMSL library [8] and in a second stage these values were used by Herrera and Gómez [9] to perform a least squares refinement for nonlinear functions (a net search algorithm) as described by Bevington [10]. The coefficients thus obtained are presented in the appendix. Another study and criticism of the Gaussian fitting coefficients can be found in the work by Weickenmeier and Kohl [11].

The values obtained for the Gaussian coefficients are presented in Appendix A.

The potential *V* acting on an electron, due to a single atom, is related to the atomic scattering factor by means of

$$V = \frac{-2\pi\hbar^2}{m} \mathcal{F}^{-1}(f(U)) \tag{7}$$

and it will prove useful to express this in terms of the so called "interaction constant"

$$\sigma = \frac{2\pi m\lambda}{h^2} \tag{8}$$

as

$$V = -\frac{\lambda}{\sigma} \mathcal{F}^{-1}(f(U)) \tag{9}$$

where  $\mathcal{F}^{-1}$  represents the inverse Fourier transform. The reason for this small change is that in the multislice calculations the quantity of interest is  $\sigma V$ . Here it is assumed that an electron with (relativistically corrected) mass m, wavelength  $\lambda$  and of energy E is incident upon a scattering atom. It should be noticed that the previous Fourier transforms are three-dimensional.

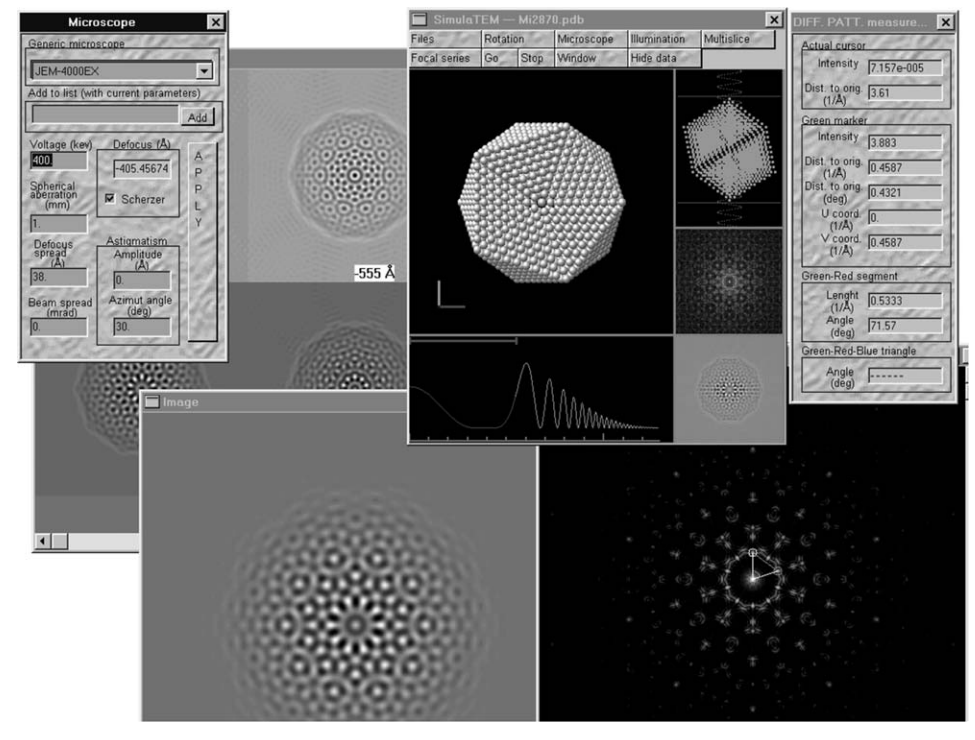
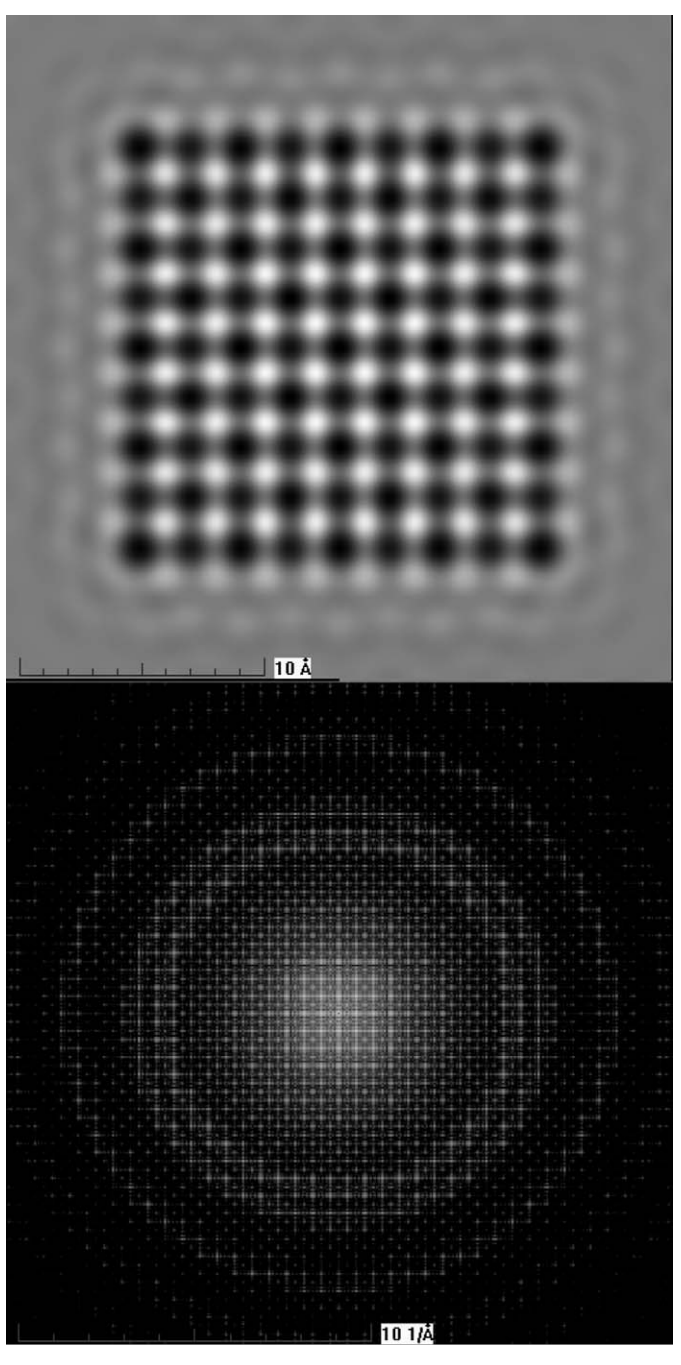


Fig. 1. A collage of the main windows in the SimulaTEM program. See text for an explanation.

Using the Gaussian coefficients we have that

$$V = \frac{-\lambda}{\sigma} \mathcal{F}^{-1} \left( \sum_{i=1}^{5} a_i \exp(-b_i U^2) \right)$$
$$= \frac{-\lambda}{\sigma} \sum_{i=1}^{5} a_i \mathcal{F}^{-1} (\exp(-b_i U^2))$$



**Fig. 2.** Image and diffraction pattern for a small gold particle composed of 366 atoms. The electron microscope simulated was a JEOL 4000EX running at 400 kV; the chromatic aberration coefficient was  $C_c = 1.4 \,\mathrm{mm}$ , the spherical aberration coefficient used was  $C_s = 1 \,\mathrm{mm}$ , the defocus was 40.6 nm, the energy spread for the microscope was set to 1.6 eV and the aperture diameter was  $10.94 \,\mathrm{nm}^{-1}$ . The aperture was centered at reciprocal space origin. For the multislice calculations slices separated by  $0.2 \,\mathrm{nm}$  were used.

$$= \frac{-\lambda}{\sigma} \sum_{i=1}^{5} \frac{a_i \pi \sqrt{\pi}}{b_i^{3/2}} \exp\left(\frac{-\pi^2 r^2}{b_i}\right)$$

$$= \sum_{i=1}^{5} A_i \exp(-D_i r^2)$$
(10)

where we have used

$$A_i = \frac{-\lambda}{\sigma} \frac{a_i \pi \sqrt{\pi}}{b_i^{3/2}}$$

$$D_i = \frac{\pi^2}{b_i} \tag{11}$$

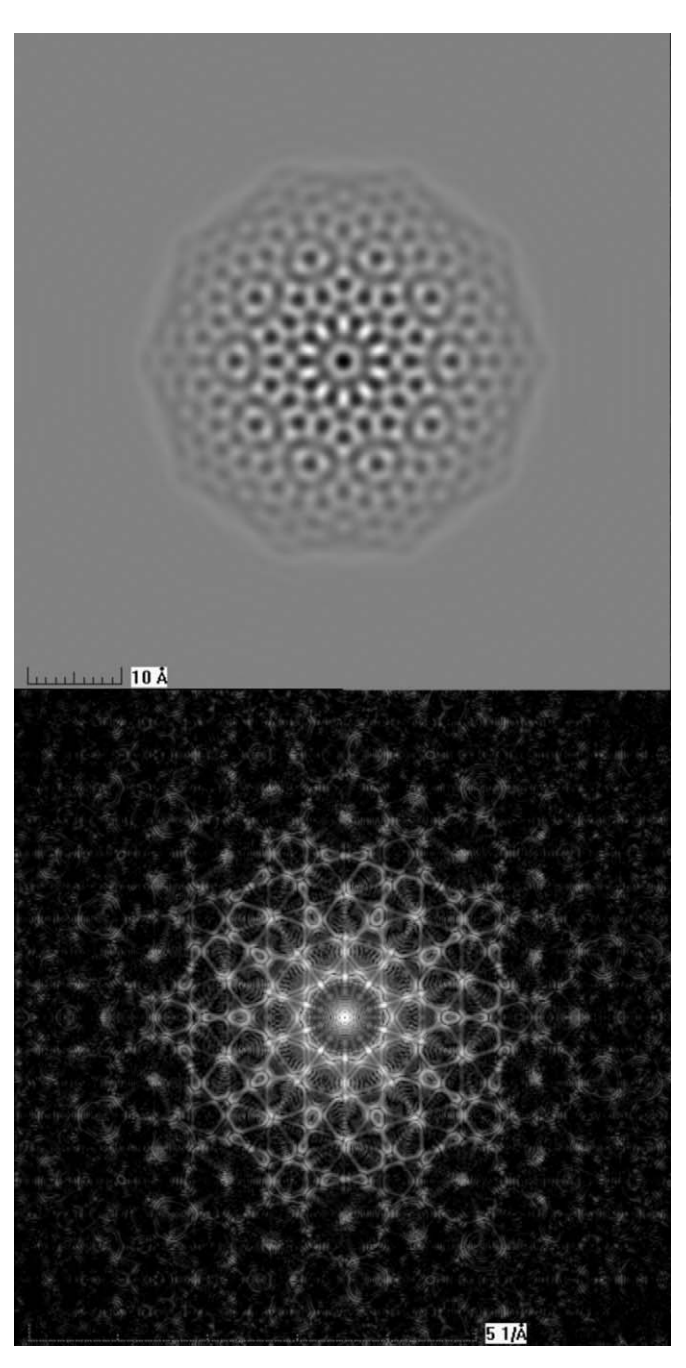


**Fig. 3.** Image and diffraction pattern for a Mackay gold icosahedron with 2869 atoms. Microscope parameters are the same as in Fig. 2.

If the atom is located at  $(x_j, y_j, z_j)$  and defining  $\alpha$  by means of

$$r^{2} = (x - x_{j})^{2} + (y - y_{j})^{2} + (z - z_{j})^{2} = \alpha^{2} + (z - z_{j})^{2}$$
(12)

then the projected potential evaluated at (x, y) can be obtained by integrating along the slice width and

$$V_p^n = \int_{z_{n-1}}^{z_n} dz \sum_{i=1}^5 A_i \exp(-D_i \alpha^2) \exp(-D_i (z - z_j)^2)$$
  
=  $\sum_{i=1}^5 A_i \exp(-D_i \alpha^2) \int_{z_{n-1}}^{z_n} \exp(-D_i (z - z_j)^2) dz$  (13)

The integral

$$I = \int_{z_{m-1}}^{z_n} \exp(-D_i(z - z_j)^2) dz$$
 (14)

can be evaluated by standard means yielding

$$I = \left(\frac{1}{\sqrt{2}\sqrt{D_i}}\right) \left[\sqrt{2\pi}Q(\sqrt{2}\sqrt{D_i}(z_n - z_j)) - \sqrt{2\pi}Q(\sqrt{2}\sqrt{D_i}(z_{n-1} - z_j))\right]$$

$$= \left(\frac{\sqrt{\pi}}{\sqrt{D_i}}\right) [Q(\sqrt{2D_i}(z_n - z_j)) - Q(\sqrt{2D_i}(z_{n-1} - z_j))]$$
 (15)

where Q is the function

$$Q(x) = \frac{1}{\sqrt{2\pi}} \int_{-\infty}^{x} \exp\left(-\frac{w^2}{2}\right) dw \tag{16}$$

Q is related to the error function

$$\operatorname{erf}(x) = \frac{2}{\sqrt{\pi}} \int_0^x \exp(-w^2) \, dw \tag{17}$$

by means of

$$\operatorname{erf}(x) = 2Q(x\sqrt{2}) - 1$$
 (18)

(see [12]). The reason for using Q instead of the more familiar erf is that below we use a simple approximating formula for Q.

Putting the various components together we have that

$$V_p^n = \sum_{i=1}^5 \frac{A_i}{D_i} \sqrt{\pi} \exp(-\alpha^2 D_i) [Q(\sqrt{2D_i}(z_n - z_j)) - Q(\sqrt{2D_i}(z_{n-1} - z_j))]$$
(19)

and, finally

$$V_p^n = \frac{-\lambda}{\sigma} \sum_{i=1}^5 \frac{a_i}{b_i} \exp\left(\frac{-\pi^2 \alpha^2}{b_i}\right) [Q(\sqrt{2D_i}(z_n - z_j)) - Q(\sqrt{2D_i}(z_{n-1} - z_j))]$$
(20)

This last expression gives the projected potential in a given slice due to a single atom. The potential due to all the atoms is calculated by adding the potentials from the various atoms.

Notice that, unlike some approaches in the literature such as [13,14], we have taken into account explicitly the (finite) thickness of the slice, some authors integrate from minus infinity to plus infinity or over a unit cell in order to simplify the expressions

The function Q has been approximated by the so-called "rational approximation" [12]:

$$Q(x) = 1 - \frac{1}{2}(1 + d_1x + d_2x^2 + d_3x^3 + d_4x^4 + d_5x^5 + d_6x^6)^{-16} + \varepsilon(x)$$
(21)

and where it is known that  $\varepsilon(x) < 1.5 \times 10^{-7}$ .

The resulting coefficients are presented in Table A1 in Appendix A.

## 4. Simulation of the microscope

The effect of the objective lens has been implemented in the standard way [15].

If the wave function after the specimen is  $\phi_-(x,y)$ , the effect of the microscope optics is given by means of a function T(x,y) that acts convolutively to produce the wavefunction  $\phi(x,y)$  after the objective lens as

$$\phi(x, y) = T(x, y) * \phi_{-}(x, y)$$
 (22)

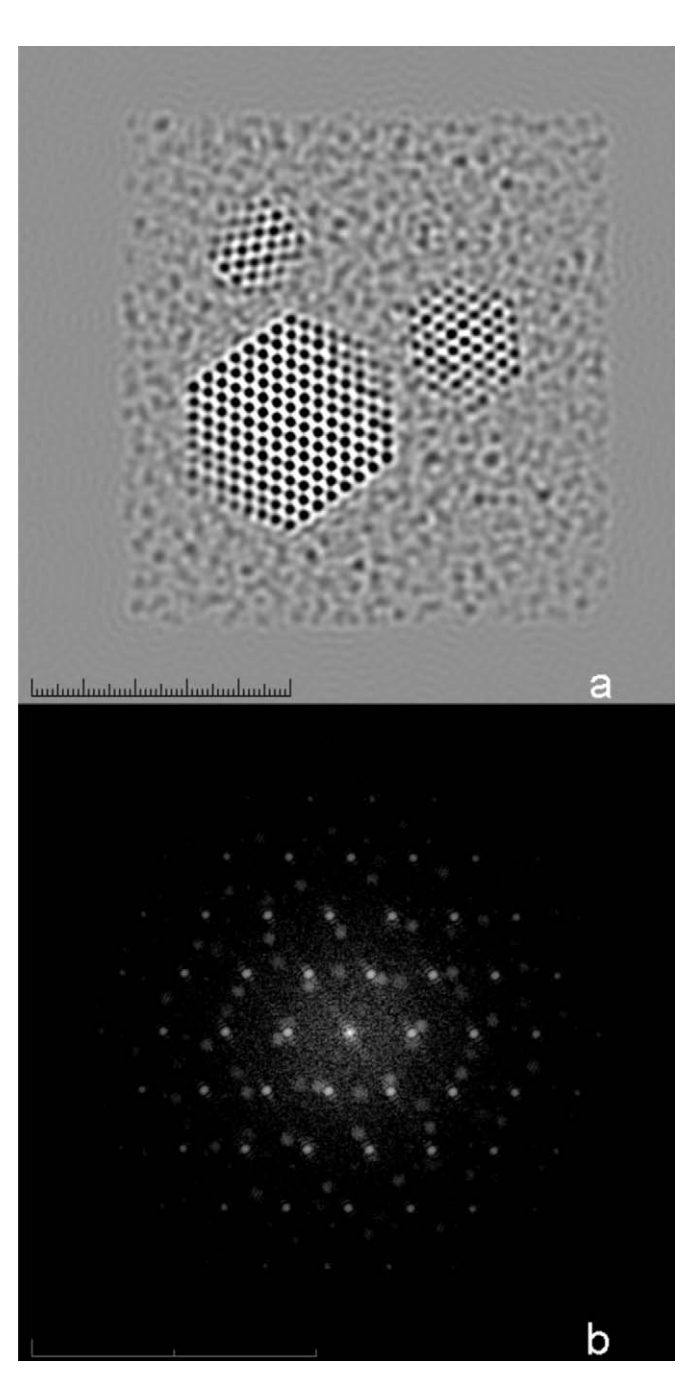


**Fig. 4.** SimulaTEM calculations for several particles on an amorphous substrate. Microscope parameters are the same as in Fig. 2.

or, in reciprocal space, as

$$\hat{\phi}(u,v) = \hat{T}(u,v) \cdot \hat{\phi}_{-}(u,v) \tag{23}$$

The function  $\hat{T}(u, v)$  is known as the transfer function for the microscope.

The observed image recorded (I(x,y)) is the modulus squared of  $\phi_+(x,y)$  so

$$I(x,y) = |\phi(x,y)|^2 \tag{24}$$

A linear approximation can be used in this quadratic expression for the purpose of clarifying the effect of the transfer function on the contrast, this requires in turn that we use a weak phase object approximation in which the terms  $e^{-i\sigma V_p(x,y,z)}$  are approximated to

$$\phi = (1 - i\sigma V_p(x, y))e^{2\pi ikz} \tag{25}$$

Within these approximations, the amplitude leaving the sample will be,

$$\hat{\phi} = \hat{T}(U)(\delta(U) - i\sigma\hat{V}_p(U)) \tag{26}$$

so the Fourier transform  $\hat{I}(U)$  of the intensity distribution will be given by

$$\hat{I}(U) = \delta(U) + \hat{T}(U)(-i\sigma\hat{V}_{p}(U)) + \hat{T}^{*}(-U)(i\sigma\hat{V}_{p}^{*}(-U))$$
(27)

where the nonlinear terms have been neglected. In terms of the Fourier transform of the contrast (r) = l(r) - 1 we have, finally, that

$$\hat{c}(U) = -2i\sigma \hat{V}_{p}^{r}(U)$$

However, it must be stressed that in SimulaTEM this linear imaging approximation is not used.

A defocus by an amount z can be represented, in real space, by convolution with

$$T(x,y) = e^{-\pi i(x^2 + y^2)/\lambda z}$$
 (28)

or, in reciprocal space, by multiplication by

$$e^{-\pi i \Delta (u^2 + v^2)/k}$$
 (29)

whereas an astigmatism can be simulated with

$$e^{-\pi i/2kA(2(a \cdot U)^2 - |U|^2)} \tag{30}$$

where A gives the amount of astigmatism and a is a unit vector specifying the direction of the astigmatism. For the spherical aberration, the contribution to the transfer is

$$e^{-\pi i/2k(\zeta_s\lambda^2|U|^4)} \tag{31}$$

where  $C_s$  is the spherical aberration coefficient. No other aberrations have been considered. The whole transfer function is (for perfectly coherent conditions) then

$$\hat{T}(U) = B(u, v)e^{-\pi i \Delta |U|^2/k}e^{-\pi i /2kA(2(a \cdot U)^2 - |U|^2) - \pi i /2k(C_s \lambda^2 |U|^4)}$$

$$= B(u, v)e^{-\pi i /k(\Delta |U|^2 + 1/2A(2(a \cdot U))^2 - |U|^2) + 1/2(C_s \lambda^2 |U|^4))}$$
(32)

*B* represents the aperture function, that is, a function that has a value of 1 inside the aperture and 0 outside.

Putting all the terms together we have that

$$\hat{c}(U) = B(u, v)\sin\left(\frac{-\pi}{k}\left(\Delta(u^2 + v^2) + \frac{1}{2}A(2(a \cdot U)^2 - |U|^2) + \frac{1}{2}(C_s\lambda^2|U|^4)\right)\right)$$
(33)

Following Spence [16] we have considered the effect of spread of defocus and beam divergence by means of envelope functions. For the focus spread we have multiplied the transfer function by

$$\exp\left(-\frac{1}{2}\pi^2\delta^2\theta^4/\lambda^2\right) \tag{34}$$

where  $\delta$  is the standard deviation for the focus values and  $\theta$  is the scattering angle.

The effect of beam divergence has been included as

$$A(|U|) = \exp(-\pi^2 u_0^2 q) \tag{35}$$

where

$$q = (C_s \lambda^3 |U|^3 + \lambda \delta |U|)^2 \tag{36}$$

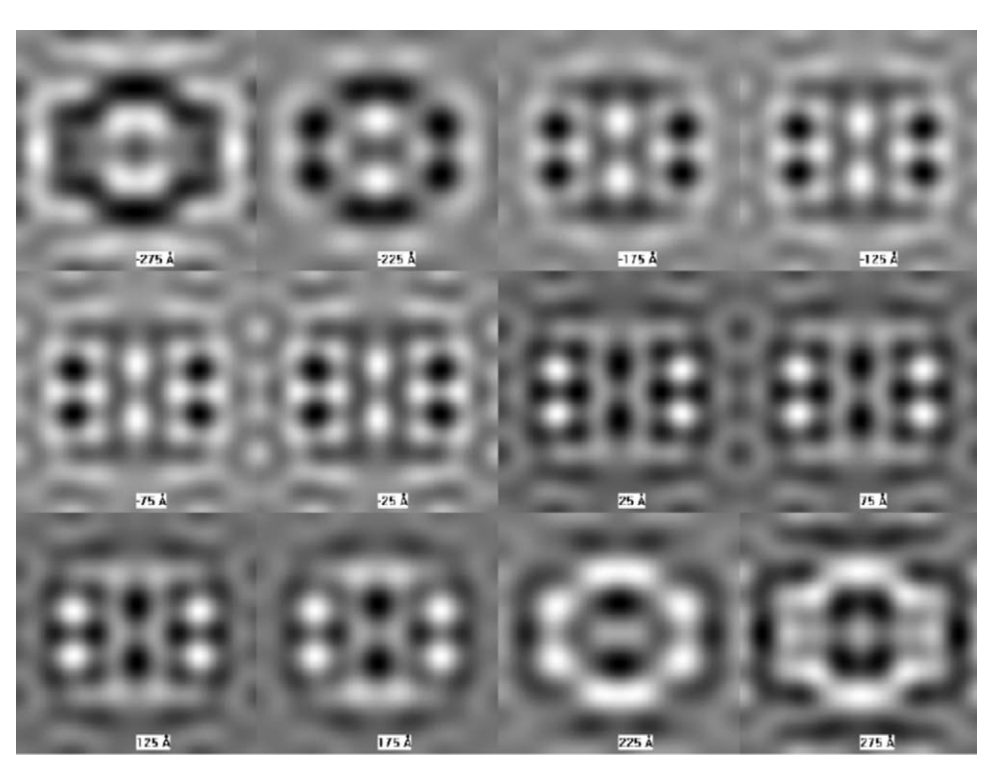


Fig. 5. Focal series around Scherzer defocus for a C60 cluster. Microscope parameters are the same as in Fig. 2.

The intensity distribution from the electron source is assumed to be a Gaussian of the form

$$\exp\left(-\frac{u^2}{u_0^2}\right) \tag{37}$$

which will attain half its height at u where

$$\exp\left(-\frac{u^2}{u_0^2}\right) = \frac{1}{2} \tag{38}$$

$$\frac{u}{u_0} = \ln(2)^{1/2} \tag{39}$$

so, for the spread angle  $\theta_c$ , converted to reciprocal quantity in the usual way by means of

$$u \approx \frac{\theta_c}{\lambda} \tag{40}$$

we have

$$\theta_c = \lambda u_0 \ln(2)^{1/2} \tag{41}$$

and  $u_0$  and  $\theta_c$  are measures of illumination spread.

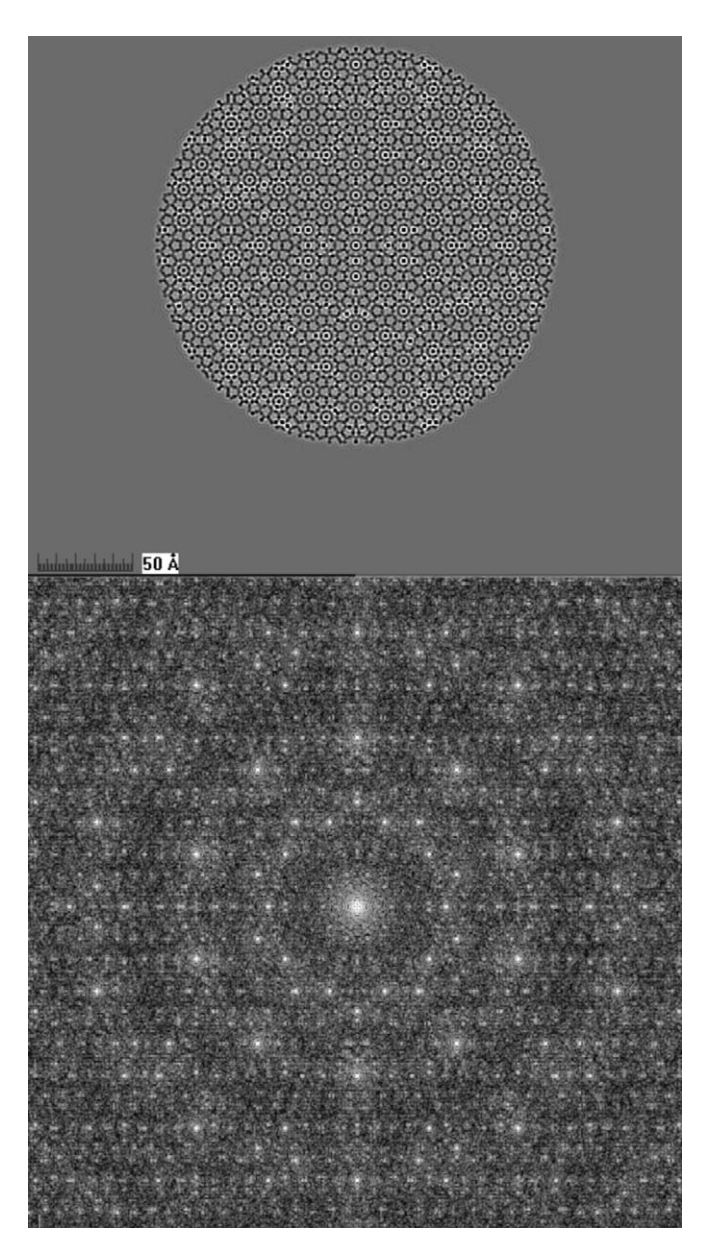


**Fig. 6.** An Al–Mn quasicrystal generated analytically. Microscope parameters are the same as in Fig. 2.

Strictly speaking this approach requires several approximations such as [15]:

- the so-called weak phase object approximation.
- that the effective source intensity distribution is symmetric and normalized to unit intensity.
- that different contributions from the source are mutually incoherent, but near coherent (small source sizes and narrow energy spread).
- the defocus distribution is assumed to be symmetric and normalized.

But we have introduced them here only for the purpose of easily incorporating the effects of partial coherence (beam divergence and focal spread); in the program we are not using the weak-phase object approximation nor the linear imaging approximation.

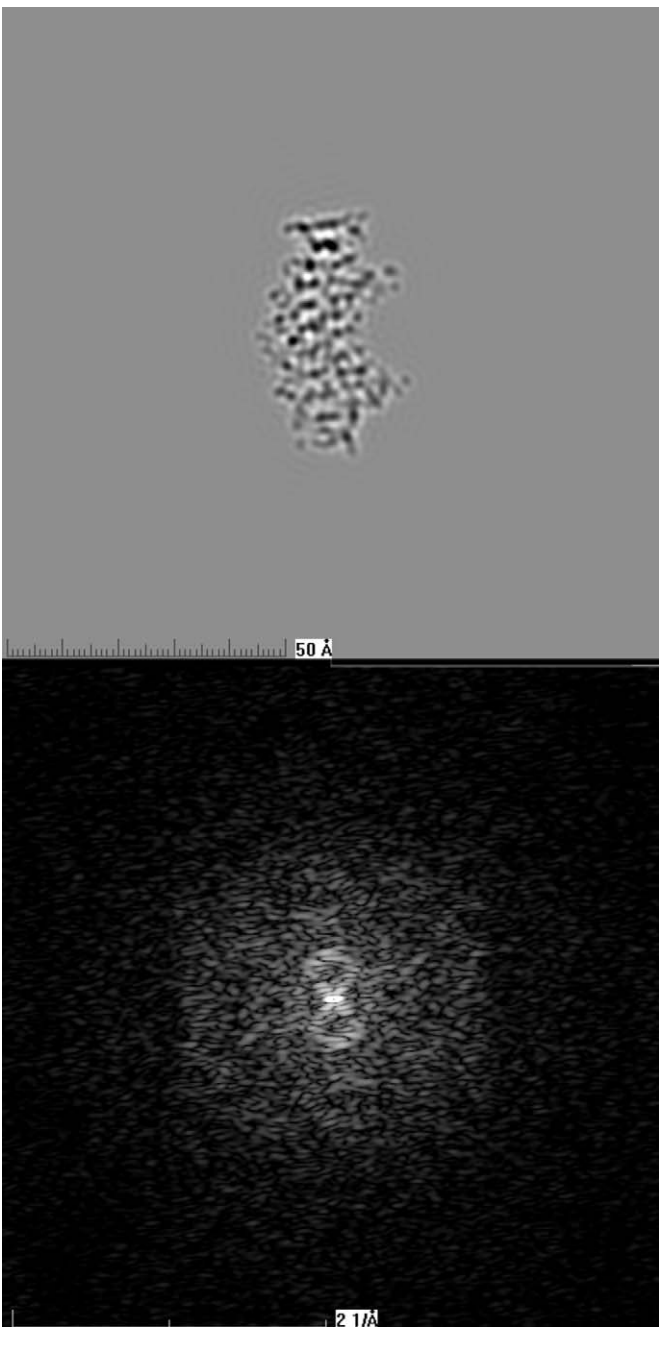


**Fig. 7.** A BDNA molecule oriented with the helix axis normal to the electron beam. There are 566 atoms in the sample. Microscope parameters are the same as in Fig. 2.

## 5. Implementation and examples

All the transforms and convolutions were calculated using the Fast Fourier Transform (see [17,4]) and the program includes a C++ coded floating point FFT routine.

Among the facilities included are the possibility of rotating the sample in the program and full focal-series capabilities (see below for an example).

SimulaTEM accepts for input both pdb (Brookhaven Protein Database) and Xmol xyz files.

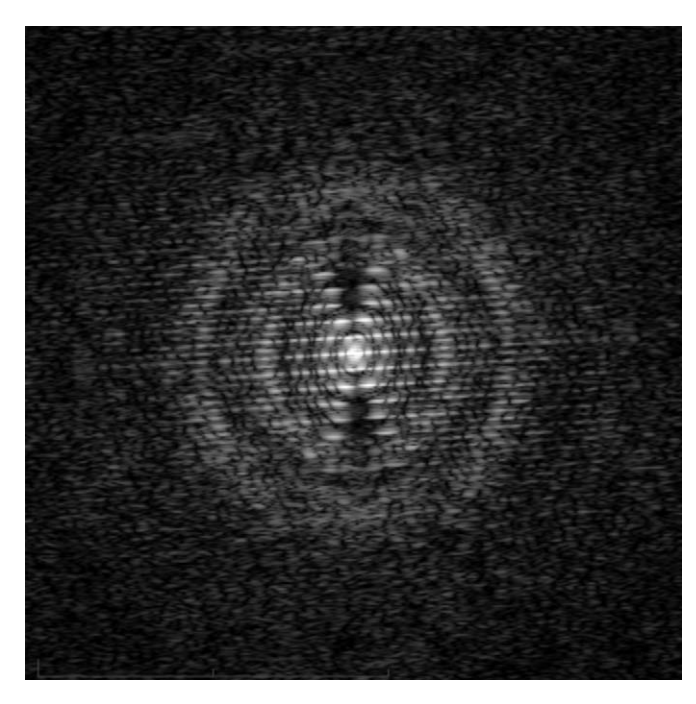
All the examples were run under a set of standardized conditions: the electron microscope simulated was a JEOL 4000 EX running at 400 kV, the spherical aberration coefficient used was  $C_s = 1$  mm, the defocus (except in the focal series) was 40.6 nm, the energy spread for the microscope was set to 1.6 eV and the aperture diameter was  $10.94 \, \mathrm{nm}^{-1}$ . The aperture was centered at reciprocal space origin. For the multislice calculations slices separated 0.2 nm were used.

In Fig. 1 we show the general layout of the user interface. In the main window the user can see a drawing of the structure, a schematic representation of the sample in side view displaying the number and position of the slices, a thumbnail of the image (for one slice) and the corresponding diffraction pattern. The phase and amplitude contrast transfer functions are presented in the lower portion of the window and the aperture extent is indicated. The menus for the various calculations (single image, focal series) are also in this window. In the same figure the microscope window (holding the microscope parameters), the measurement windows and the focal series window can be appreciated together with the image and diffraction pattern windows.

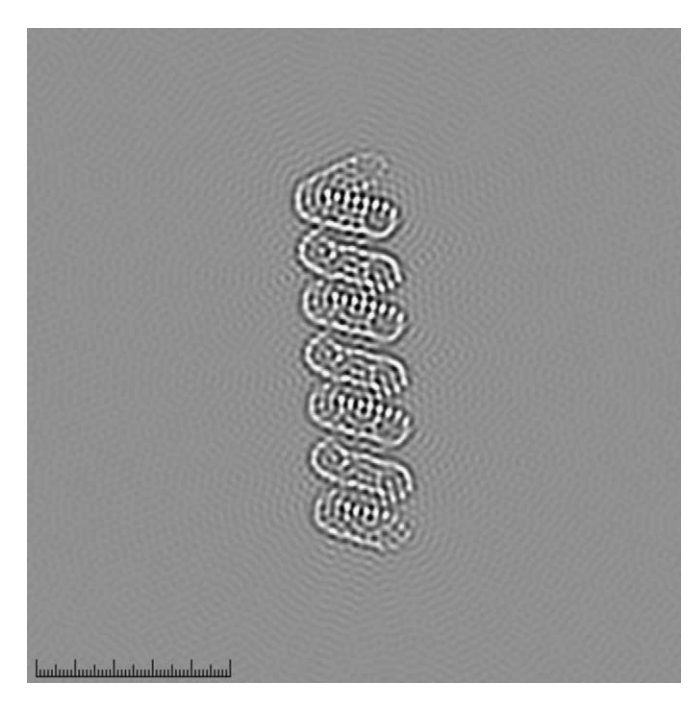
In Fig. 2 we show the behavior of the program for a finite crystal. This example is intended to show that the program can do the usual tasks such as simulating crystals, in this example the otherwise periodicity is interrupted by the finite size of the particle. This is the image from a gold crystal in [100] orientation for 400 keV, Scherzer defocus and 1 mm spherical aberration. The corresponding diffraction pattern is shown with the contrast greatly enhanced.

Fig. 3 presents the image and diffraction pattern for a gold Mackay icosahedron [18]. The parameters are the same as for the previous figure. This is an example meant to show how a polycrystal can be simulated, the icosahedron is basically a multiply twinned f.c.c crystal.

Fig. 4 illustrates the calculation from several hexagonally shaped gold f.c.c. [111] crystals on an carbon amorphous substrate. The substrate was modeled as a random array of carbon atoms subject to the restriction that no two of them were closer than an atomic distance in crystalline graphite. In this way we see that we can



**Fig. 9.** Diffraction pattern from a carbon naotube with 2710 atoms. Microscope parameters are the same as in Fig. 2.



**Fig. 8.** Image of a carbon naotube with 2710 atoms. Microscope parameters are the same as in Fig. 2.

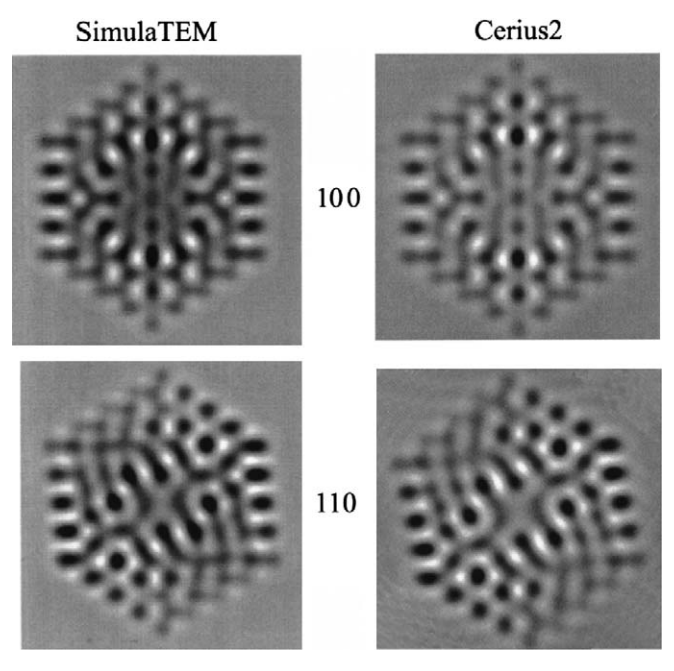


**Fig. 10.** Cerius 2 and SimulaTEM images for a gold multiply twinned particle with 309 atoms. Picture courtesy of J. Ascencio.

**Table A1**Gaussian coefficients.

Z	a1	a2	аЗ	a4	a5	<i>b</i> 1	b2	b3	<i>b</i> 4	b5
H-1	0.1671	0.2563	0.0393	0.0596	0.0078	6.0583	20.3093	70.2973	1.3067	0.0102
He-2	0.1227	0.1579	0.0089	0.0926	0.0358	14.1248	5.0260	36.9356	1.6644	0.2832
Li-3	0.7762	0.0644	0.2118	1.0882	1.1218	16.2591	0.3254	2.5832	85.6315	80.5508
Be-4	0.0197	1.5392	0.2990	0.1283	1.0548	0.0243	52.2488	4.1219	0.8202	15.6590
B-5	0.4441	0.0720	1.1248	0.9794	0.1695	5.2074	0.2374	15.0436	44.6563	1.4821
C-6	1.0392	0.5255	0.2246	0.0861	0.6326	15.4799	42.5178	1.5692	0.2390	5.5375
N-7	0.9271	0.4702	0.0611	0.5487	0.2047	11.0027	32.1051	0.1308	3.8783	1.0445
0-8	0.7118	0.2561	0.6403	0.2767	0.0983	11.5989	29.7811	4.4138	1.3555	0.2103
F-9	0.2917	0.6223	0.6257	0.1632	0.0983	1.2215	10.6435	3.9383	27.6191	0.1846
Ne-10	0.1250	0.1644	0.4632	0.5452	0.3541	0.2162	22.1640	9.1228	3.9942	1.3653
Na-11	1.0417	0.6892	0.1996	1.2693	1.5679	12.4203	2.1683	0.3158	131.093	62.9926
Mg-12	0.6946	0.1704	2.0512	1.8009	0.4841	5.5229	0.2462	77.5613	24.3472	1.5433
Al-13	0.5217	0.1944	0.7933	2.4057	1.9661	1.6064	0.2596	6.3070	24.1637	78.1749
Si-14	1.8563	0.8424	0.4860	2.4408	0.1954	61.6656	5.6894	1.4450	19.8377	0.2430
P-15	2.2615 1.0234	1.8096	0.4399	0.7882	0.1817	15.0540	45.2182	1.2297	4.6428	0.2100
S-16	0.5037	1.2139 0.2446	0.4932 0.9581	2.1986 1.9974	0.2293	5.5511 1.4730	41.8781 0.2489	1.4617 36.5515	15.4568 14.2213	0.2477 5.4897
Cl-17	0.8942	1.9768	0.1070	1.9974 1.1841	1.1525	1.4730 3.4094	0.2489 9.8793	0.0763	27.1976	5.4897 0.7596
Ar-18		0.8878		2.4758	0.4159	0.3315				
K-19	0.3371 0.6173		2.5273 1.6416	2.4758	2.6079	1.6400	2.2665 0.2468	9.0998	101.835	85.6052
Ca-20 Sc-21	1.7260	0.2885 2.3637	0.2989	4.1911	5.1654 0.6974	5.6109	20.8270	5.5582 0.2446	18.0165 83.9145	86.4565 1.6783
	1.7508									
Ti-22 V-23	0.3225	2.4914 2.4858	0.7528 0.8123	0.3070 2.9576	3.4557 1.7139	5.5714 0.2477	22.1798 22.3821	1.6591 1.6916	0.2448 80.5410	82.7864 5.4920
V-23 Cr-24	1.6778	0.8399	1.9966	0.3165	2.1247	5.2661	1.6077	20.1030	0.2328	82.4882
Mn-25	0.8970	2.3635	0.3296	1.6190	2.1247	1.6174	74.1583	0.2464	5.2368	21.2391
Fe-26	0.9641	0.3397	2.1773	2.0815	1.5664	1.6217	0.2341	21.1950	70.7154	5.3081
Co-27	2.0668	1.4921	0.3477	0.9572	1.9833	19.7711	5.0028	0.2315	1.5690	68.3097
Ni-28	1.8929	1.9648	0.9275	1.4477	0.3288	64.4272	18.2869	1.4276	4.5981	0.2091
Cu-29	1.4292	0.9819	1.2946	0.3448	1.5426	4.7334	1.4435	71.8921	0.2258	18.3285
Zn-30	1.5439	1.7832	1.0213	1.3392	0.3722	62.0393	18.4854	1.4805	4.7984	0.2250
Ga-31	1.1303	1.3643	0.4097	2.3827	1.8133	1.5844	5.5819	0.2414	22.0962	76.1567
Ge-32	2.6367	1.3324	0.4029	1.0846	1.9141	19.7849	5.2086	0.2298	1.4807	64.0820
As-33	2.6865	1.2748	0.3853	1.0297	1.9382	16.7493	4.7274	0.2125	1.3530	50.8067
Se-34	1.1632	1.0534	2.7186	0.3958	1.8692	4.6405	1.3573	14.6754	0.2104	42.7844
Br-35	2.7310	1.6535	1.2619	0.4015	1.0081	13.8481	38.1205	4.6020	0.2098	1.2880
Kr-36	2.7163	1.2399	1.6285	0.3668	0.9433	12.0800	4.0874	32.8791	0.1977	1.1280
Rb-37	0.4637	0.8657	5.7261	3.6288	0.9655	0.2420	1.1826	106.6006	11.2431	4.0022
Sr-38	3.0069	1.7449	6.5739	1.1999	0.5062	15.5935	6.2286	92.0409	1.5694	0.2374
Y-39	2.2413	3.2281	1.0127	5.6088	0.4937	5.5921	18.4113	1.3346	83.3015	0.2361
Zr-40	0.5090	3.5092	1.0341	4.5954	2.4670	0.2341	20.5167	1.3658	82.1291	5.6990
Nb-41	2.5661	1.0335	3.3941	3.1423	0.5083	5.5531	1.3433	19.7223	81.3820	0.2265
Mo-42	2.6130	3.2953	0.5370	1.0379	2.7607	5.4630	19.1458	0.2343	1.3838	78.5426
Tc-43	2.6630	3.4140	1.0671	0.5563	3.1287	5.4012	19.7416	1.4296	0.2352	73.4475
Ru-44	2.2004	3.0256	1.0724	0.5667	2.6688	73.3132	18.0130	1.4301	0.2345	5.2267
Rh-45	2.6577	2.9019	0.5614	1.0653	2.0332	4.9678	17.0684	0.2387	1.3751	70.7299
Pd-46	2.5413	2.1993	0.5259	0.9384	1.3647	11.3044	4.0573	0.2084	1.2112	37.2810
Ag-47	1.8384	2.3312	2.7903	1.0877	0.6126	65.8402	16.6748	4.4648	1.6473	0.2208
Cd-48	2.6685	2.1385	2.6325	1.1951	0.5889	16.8333	62.4892	4.7990	1.4484	0.2229
In-49	2.6440	3.1524	2.6224	0.6344	1.3668	5.1688	20.1585	74.9156	0.2357	1.6104
Sn-50	2.5195	1.3462	3.4633	0.6255	2.8933	4.8336	1.5451	18.9352	0.2287	65.4807
Sb-51	1.3188	3.0205	2.4045	0.6121	3.6070	1.4835	54.8259	4.4975	0.2180	17.3120
Te-52	1.3955	2.2768	3.7388	0.6198	2.9538	1.4883	4.5170	16.3599	0.2185	48.3219
I-53	2.1533	3.8460	1.4118	2.8707	0.6161	4.3665	15.0853	1.4545	42.9408	0.2133
Xe-54	3.9274	2.0577	2.8684	0.5981	1.3354	13.5943	3.9880	37.9476	0.2036	1.3570
Cs-55	-0.668	5.5571	7.4047	3.1363	0.9480	116.2077	16.1736	130.5351	3.0163	0.3151

Ba-56	4.9425	1.7545	1.5258	0.6531	9.2106	12.8126	4.4419	1.4331	0.2207	94.6924
La-57	2.2875	4.9018	8.1591	0.6608	1.5861	4.8334	14.9771	85.6484	0.2146	1.4768
Ce-58	4.7170	2.3595	0.6537	7.7855	1.6735	15.2154	4.9884	0.2064	85.0290	1.4784
Pr-59	1.4556	7.9891	0.6898	2.1328	4.4767	1.2831	88.5581	0.2415	4.5188	12.9865
Nd-60	2.2056	1.5448	0.6045	4.2878	7.6905	4.3697	1.2638	0.1862	13.0088	85.9794
Pm-61	2.2450	1.6102	0.6410	4.0937	7.4307	4.5693	1.3109	0.1971	13.2392	86.9048
Sm-62	1.6045	2.2588	0.6559	7.1214	4.0662	1.3015	4.4541	0.2003	87.0279	13.5148
Eu-63	3.8096	2.3219	1.6964	0.6868	6.9420	13.7564	4.7841	1.3480	0.2086	87.7834
Gd-64	3.8749	2.7972	0.6963	1.7629	6.0304	17.0522	5.2416	0.2074	1.3628	83.1903
Tb-65	0.6498	1.6649	3.5427	2.4159	6.5029	0.1991	1.2318	13.7926	4.5019	83.3409
Dy-66	2.4738	6.1335	1.7776	0.6959	3.4270	4.8493	85.4899	1.3396	0.1969	14.8320
Ho-67	1.8098	0.7445	3.6104	5.2182	2.9453	1.3701	0.2133	19.1664	82.8910	5.4014
Er-68	2.5628	1.7106	0.6949	3.2366	5.7506	4.6974	1.2429	0.1955	15.0116	83.5002
Tm-69	1.7198	5.5250	2.6164	0.7377	3.1045	1.2690	83.9429	4.8412	0.2077	15.5758
Yb-70	0.7372	3.0525	2.5715	1.7210	5.3674	0.2046	15.5384	4.7264	1.2520	83.1496
Lu-71	1.8020	0.7869	3.4122	2.8794	4.5570	1.3302	0.2139	20.1865	5.2475	81.9125
Hf-72	3.9427	3.6345	1.8274	0.8219	2.9228	77.0186	20.8925	1.3673	0.2205	5.3852
Ta-73	0.8327	3.7562	2.9475	1.8085	3.4870	0.2208	20.3697	5.3281	1.3533	72.6260
W-74	0.8296	3.1549	2.9461	1.7764	3.8167	0.2160	68.5278	5.1589	1.3249	19.3610
Re-75	3.7785	2.9524	1.7648	0.8541	2.8968	18.5062	5.1211	1.3309	0.2202	64.2221
Os-76	3.7057	2.8390	0.8161	1.6999	2.8998	16.5584	58.1703	0.2070	1.2417	4.7727
Ir-77	1.6972	0.8463	3.6636	2.5472	2.9490	1.2614	0.2126	16.3008	56.7139	4.7925
Pt-78	3.3756	1.9202	1.6818	0.8701	2.9537	15.0204	53.3690	1.2708	0.2162	4.7357
Au-79	0.8239	1.6166	3.3603	1.8342	2.9307	0.2015	1.1760	13.8414	50.2016	4.4106
Hg-80	3.3429	1.9700	1.6900	0.9145	3.0414	14.9551	51.2359	1.3061	0.2209	4.7166
Tl-81	2.4154	3.7157	1.7410	3.2675	0.9469	66.8719	17.5708	1.3552	4.9322	0.2258
Pb-82	1.7524	0.9381	2.7140	3.9155	3.2667	1.3349	0.2202	61.8636	17.4937	4.8583
Bi-83	3.1838	4.1659	0.9545	3.0415	1.7389	4.7027	16.9894	0.2215	57.5155	1.3394
Po-84	3.0981	1.6868	0.9255	4.3552	3.2795	4.4110	1.2698	0.2119	15.9020	51.2527
At-85	4.4662	3.0129	3.3002	1.7249	0.9516	15.3682	4.4009	46.5313	1.3060	0.2154
Rn-86	4.6212	2.9312	1.6640	0.9154	3.3501	14.2812	4.1129	1.2241	0.2046	42.0807
Fr-87	6.1052	-0.314	3.0127	8.0414	1.3720	11.2782	77.9414	2.3975	88.8819	0.3074
Ra-88	2.7718	1.5937	9.1922	5.8530	0.8400	3.6817	1.0968	88.4473	13.4212	0.1798
Ac-89	3.1041	1.9460	5.7975	8.4287	1.0283	4.8348	1.4065	16.1952	84.2792	0.2249
Th-90	1.0606	6.1558	2.1278	7.2005	3.5299	0.2277	19.1693	1.5027	83.1842	5.4688
Pa-91	3.3789	2.1098	7.2538	1.0752	5.6246	5.2199	1.4957	83.0861	0.2301	17.2570
U-92	2.1845	1.0774	5.4600	3.5175	6.8170	1.5185	0.2261	17.5536	5.3832	83.9202
Np-93	1.0605	5.3227	2.1706	6.4498	3.6607	0.2209	17.6673	1.4668	82.6385	5.3317
Pu-94	5.0018	3.3635	1.0312	2.0638	6.5815	15.0396	4.7751	0.2118	1.3854	83.8012
Am-95	2.1135	3.4848	1.0497	4.8075	6.2502	1.4178	4.8644	0.2126	15.4049	83.6486
Cm-96	2.3024	3.8828	1.0947	5.5030	4.8629	1.5087	5.4420	0.2212	82.1515	18.6116
Bk-97	3.9615	4.7078	1.1034	5.2136	2.3627	5.5156	19.1735	0.2330	82.2191	1.5087
Cf-98	3.9176	5.1700	2.3428	1.0923	4.4169	5.3363	75.3300	1.4895	0.2161	18.2466

simulate not only crystals and amorphous bodies but their juxtaposition, a very common occurrence.

The focal series capabilities are illustrated in Fig. 5 in which a focal series is shown for a C60 cluster. As expected SimulaTEM can provide focal series with focus steps given by the user.

Quasicrystals can be easily simulated, in Fig. 6 we show the image and diffraction pattern of an Al-Mn quasicrystal generated by the analytic methods of Naumis and Aragón [19]. This examples shows the behavior of the program under quasiperiodic objects, of current importance.

Of particular interest for some users might be the possibility of simulating images of large molecules, such as the BDNA molecule shown in Fig. 7. This molecule was downloaded from the Protein Data Bank [20] and the simulation parameters are the same as in the other simulations in this paper. The sample consisted of 566 atoms. With this example it is emphasized that in principle any object composed of atoms could be simulated.

Carbon nanotubes provide our next example, in Figs. 8 and 9 a carbon nanotube with 2710 atoms is shown. The diffraction pattern (with a highly enhanced contrast) shows the typical X-shaped pattern. This is a carbon helicoidal structure formed by pentagonal and heptagonal rings. These rings provide the right curvature to produce a helix. The model was provided by Terrones [21]. Given the importance of nanotubes and related materials we emphasize again that all these modern materials can be simulated.

## 6. Comparison with other programs

In order to compare SimulaTEM with similar programs we downloaded the Jems student version programm by Stadelmann [22], version 3.3526U2008. The sample used was the Si1419 found in the Jems distribution; it is a cluster with 1419 Si atoms. The Jems file was edited to convert it into an \*.xyz file that could be read by SimulaTEM. In both simulations the electron microscope was a JEOL 4000EX running at 400 kV; chromatic aberration coefficient  $C_c = 1.4 \,\mathrm{mm}$ , spherical aberration coefficient  $C_s = 1 \,\mathrm{mm}$ ,  $C_5 = 0$ , defocus 40.6 nm, energy spread 1.6 eV and aperture diameter 10.94 nm<sup>-1</sup>. The aperture was centered at reciprocal space origin. For the Jems part it is assumed that the cell is triclinic with a = b = c = 4.3447 nm. All calculations were performed with a  $512 \times 512$  sampling. The beam half convergence was set to zero. The defocus spread was set to 3.8 nm. Jems took (as measured with a stopwatch) 30.0 s to compute everything. The image calculation (as measured by the very program) took 10.46 s. In SimulaTEM the same calculation took (as measured with a stopwatch, SimulaTEM does not include a built-in timer) 3.5 s. Great care was taken to ensure that, in Jems, the menu option "Imaging" was used and to choose the option "Multislice" and not "Blochwave"; Jems (unlike SimulaTEM) can also do Bloch wave calculations.

Ascencio [23], in his doctoral dissertation, briefly compared the outputs from Cerius2 and SimulaTEM for multiply twinned icosahedral gold particles in various orientations. In Fig. 10 we show these results. Visually the images from both programs are very similar (notice a 90° relative misorientation between the simulations).

## 7. Conclusions

In this work we have shown how to calculate multislice simulations of electron microscopy diffraction patterns and images for arbitrary objects. Nowhere is periodicity assumed and the calculation of projected potentials is achieved by integrating along the actual slice boundaries which are not related to any sort of unit cell. No symmetry groups are used at all. Future work contemplates the calculation for STEM configurations (certainly those not related by reciprocity to CTEM ones). With this approach nanostructures can be simulated as well as substrates, molecules boundaries etc. The program itself can be freely downloaded from [24].

## Acknowledgments

The history of this project is long. V.M. Castaño contributed to some of the original ideas in his Ph.D. dissertation. The main ideas were developed during a sabbatical leave by A.G.R. at Lehigh University which was made possible thanks to the support and kind invitation by K. Klier to whom we also owe many interesting discussions. P. Klier coded the very first attempts whereas R. Herrera in the course of his Ph.D. research wrote the first working program. Later L.M. Beltrán and A. Gómez produced SimulaTEM. Last, but not least, we wish to express our thanks to our friend and mentor M. José Yacamán without whose support this project would have never been possible. We received considerable technical assistance from S. Tehuacanero and C. Zorrilla. We are very grateful to Jorge Ascencio for permission to use his comparison of Cerius2 and SimulaTEM. Support from PAPIIT Grants IN105109-3 and CONACYT 50368.

## Appendix A. Gaussian coefficients

The resulting coefficients are shown in Table A1.

## References

- [1] J.M. Cowley, A.F. Moodie, Acta Cryst. 10 (1957) 609–619.
- [2] J. Kirkland, Advanced Computing in Electron Microscopy, Plenum Press, New York, London, 1998.
- [3] K. Ishuzuka, Microsc. Microanal. 10 (2004) 34-40.
- [4] O. Brigham, The Fast Fourier Transform and its Applications, Prentice-Hall, Englewood Cliffs. NI. 1988.
- [5] P.A. Doyle, P.S. Turner, Acta Cryst. A 24 (1968) 390.
- [6] D.T. Cromer, T.J. Waber, International Tables for X-Ray Crystallography, vol. 4, Kynoch Press, Birmingham, 1974.
- [7] K. Klier, P.Klier, A. Gómez, R. Herrera, unpublished results.
- [8] IMSL Library Reference Manual, IMS. Inc., Company, Houston, Texas, 1980.
- [9] R. Herrera, Un Algoritmo para la Simulación de Imágenes y patrones de difracción de objetos arbitrarios en Microscopía Electrónica de Alta Resolución, Ph.D. Dissertation, C.I.C.E.S.E, Ensenada, México, 1989.
- [10] P.R. Bevington, Data Reduction and Error Analysis for the Physical Sciences, McGraw-Hill, New York, 1969.
- [11] A. Weickenmeier, H. Kohl, Acta Cryst. A 47 (1991) 590-597.
- [12] M. Fogiel, Handbook of Mathematical Formulas, Tables, Functions, Graphs and Transforms, Staff of Research and Education Association, New York, 1980.
- [13] M. Pan, P. Rez, J.M. Cowley, in: Proceedings of the 47th Annual Meeting of the Electron Microscopy Society of America, 1989, pp. 478–479.
- [14] D. Van Dyck, W. Coene, Ultramicroscopy 15 (1984) 29–40.
- [15] W.O. Saxton, Computer Techniques for Image Processing in Electron Microscopy, Academic Press, New York, 1978.
- [16] J.C.H. Spence, Experimental High-resolution Electron Microscopy, Oxford University Press, Oxford, 1988.
- [17] J.W. Cooley, J.W. Tukey, Math. Comput. 19 (1965) 297–301.
- [18] A.L. Mackay, Acta Cryst. 15 (1962) 916.
- [19] G.G. Naumis, J.L. Aragón, Z. Kristallogr. 218 (2003) 397–420.
- [20] H.R. Drew, R.M. Wing, T. Takano, C. Broka, S. Tanaka, K. Itakura, R.E. Dickerson, Structure of a B-DNA dodecamer: conformation and dynamics, Proc. Natl. Acad. Sci. USA 78 (1981) 2179–2183; Protein Data Bank DOI 10.2210/pdb1bna/pdb.
- [21] H. Terrones, Private communication.
- [22] P. Stadelmann. JEMS Java Electron Microscopy Software <a href="http://cimewww.epfl.ch/people/stadelmann/jemsWebSite/jems.html">http://cimewww.epfl.ch/people/stadelmann/jemsWebSite/jems.html</a>.
- [23] J. Ascencio, Simulación de procesos de agregación de nanopartículas y su análisis mediante microscopía electrónica de alta resolución, Tesis, Universidad Autónoma del Estado de México, Toluca, México.
- [24]  $\langle$  http://www.fisica.unam.mx/personales/alfredo $\rangle$ .